Laser and Particle Beams (2012), *30*, 473–479.

doi:10.1017/S0263034612000407

Femtosecond laser ablation of brass: A study of surface morphology and ablation rate

MOHAMED E. SHAHEEN[1,2] AND BRIAN J. FRYER[1,3]

[1]Great Lakes Institute for Environmental Research, University of Windsor, Windsor, Ontario, Canada
[2]Department of Physics, Faculty of Sciences, Tanta University, Tanta, Egypt
[3]Department of Earth and Environmental Sciences, University of Windsor, Windsor, Ontario, Canada

(Received 20 March 2012; Accepted 25 April 2012)

Abstract

The interaction of near infrared femtosecond laser pulses with a Cu based alloy (brass) in ambient air at atmospheric pressure and under different laser conditions was investigated. The effects of laser fluence and number of pulses on surface morphology and ablation rate were studied using scanning electron microscopy (SEM) and optical microscopy. Ablation rates were found to rapidly increase from 83 to 604 nm/pulse in the fluence range 1.14–12.21 J/cm^2. At fluence >12.21 J/cm^2, ablation rates increased slowly to a maximum (607 nm/pulse at 19.14 J/cm^2), and then decreased at fluence higher than 20.47 J/cm^2 to 564 nm/pulse at 24.89 J/cm^2. Large amounts of ablated material in a form of agglomerated fine particles were observed around the ablation craters as the number of laser pulses and fluence increased. The study of surface morphology shows reduced thermal effects with femtosecond laser ablation in comparison to nanosecond laser ablation at low fluence.

Keywords: Brass; Femtosecond laser; Laser ablation; Scanning electron microscopy

INTRODUCTION

Femtosecond laser ablation (fs-LA) has been successfully applied in many applications that cover various scientific disciplines including medicine (Liu & Niemz, 2007; Niemz, 1998), dentistry (Neev *et al.*, 1996; Niemz *et al.*, 2004; Ji *et al.*, 2011), material science (Coyne *et al.*, 2005; Bonse *et al.*, 2001, 2002; Choi *et al.*, 2002; Couillard *et al.*, 2007), and geosciences (Freydren *et al.*, 2008; Frenandez *et al.*, 2007; Horn & von Blanckburg, 2007; Ikehata *et al.*, 2008; Poitrasson *et al.*, 2003, Shaheen & Fryer, 2011). The interactions of laser pulses with a solid material involve many processes that depend on the laser parameters (pulse width, repetition rate, fluence, wavelength, and irradiance), the physical and chemical characteristics of the target material, and on the ambient gas environment (gas pressure and gas properties) (Russo *et al.*, 2002). Therefore, an appropriate choice of the ablation conditions is necessary for each type of material in order to optimize the ablation process (Di Bernardo *et al.*, 2003). Laser pulse width is an important parameter that affects heat dissipation into the sample, plasma shielding, and ablation quality. In nanosecond laser ablation, thermal processes dominate, and the material is melted at the irradiation volume with the formation of a large heat affected zone. Large droplets of molten material are ejected and deposited on the surface as a recast layer. In addition, part of the incident laser pulse interacts with the laser-induced plasma causing a reduction in the amount of energy absorbed by the material (plasma shielding). The laser-induced plasma can interact with the target surface causing further damage and distortion of the ablated craters. The situation is different in the case of femtosecond laser pulses due to their high peak intensity. Femtosecond laser energy is rapidly deposited into a small volume of the target material on a time scale shorter than the energy relaxation time. This significantly reduces the liquid phase and thermal diffusion to the surrounding material, leading to a lower ablation threshold, reduction of molten material and negligible thermal damage, high ablation rate, and more deterministic and reproducible ablation compared to nanosecond laser.

Studies of surface modification of materials, including metals and alloys, by laser beams, together with investigations of fundamentals of laser-matter interactions are important for developing new applications (Stasic *et al.*, 2009; Latif *et al.*, 2009; Fang *et al.*, 2010; Menendez-Manjon *et al.*, 2010;

Address correspondence and reprint requests to: Mohamed E. Shaheen, Great Lakes Institute for Environmental Research, University of Windsor, Windsor, Ontario, Canada N9B 3P4. E-mail: mshaheen@uwindsor.ca

Kumar Verma, 2011; Batani, 2010). Melting and formation of a recast layer (a re-solidified molten material that deposits at the ablation crater or at the surface surrounding it) is a challenging problem to laser processing as it restricts the formation of high quality structures (Robinson & Jackson, 2006). Material processing with ultrashort laser pulses possesses unique advantages over that with longer laser pulses due to the absence of plasma shielding, a well-defined ablation threshold and a negligible heat affected zone (Zhu *et al.*, 1999). It became a preferred technique for various machining applications such as drilling, cutting, and fabrication of variety of materials, such as low melting point polymers, high thermal conductivity metals, wide band gap dielectrics, and semiconductors that are otherwise difficult to perform by conventional tools (Zheng *et al.*, 2007; Pecholt *et al.*, 2008). The use of fast flowing inert gas as a medium for ablation instead of air helps to prevent surface oxidation and improves removal of melt, particulate, and vapor from the interaction area. It also minimizes the problems that can result from the interaction of high intensity laser beams with the air and ablated material (laser-induced plasma that could affect the temporal and spatial profile of the laser beam and the subsequent degradation of the quality and precision of femtosecond laser micromachining) (Sun & Longtin, 2001). Femtosecond lasers have been applied to produce high quality microstructures in materials that have high thermal conductivity and low melting point (Perrie *et al.*, 2004; Robinson & Jackson, 2006). In this paper, we studied the ablation characteristics of a Cu based alloy (brass) in air using a 785 nm, 130 fs Ti:Sapphire laser. Holes were drilled at different laser fluence and number of pulses using a 6 mm pinhole to remove the inhomogeneous edge of the laser beam. The ablation rates and surface morphology in the fluence range from 1.14 to 24.89 J/cm^2 have been investigated using a polarized light optical microscope and SEM.

EXPERIMENTAL PROCEDURE

Laser pulses were obtained from a commercial femtosecond Ti:Sapphire laser system (Quantronix Integra C®) located at the Great Lakes Institute for Environmental Research, University of Windsor, Canada. It is a regenerative and multipass Ti:sapphire laser ablation system based on the chirped pulse amplification technique. The laser operates at its fundamental wavelength of 785 nm and can be operated at variable repetition rates from 4 to 1000 Hz. The maximum energy that can be obtained from this laser system is 2 mJ at 1 kHz and can be varied using a half wave plate and polarizer integrated in the laser system. The minimum pulse width is 130 fs and can be changed to a few picoseconds by changing the distance between the pulse compressor gratings.

The sample (SRM 1107 Naval brass B from National Institute of Standard and Technology (NIST) with chemical composition: 61.2% Cu, 37.3% Zn, 0.18% Pb, 0.037% Fe, 1.04% Sn and 0.098% Ni) was mounted on a three-dimensional computer-controlled translation stage of 1 μm resolution where ablation was conducted in ambient air. The upper surface of the sample was polished prior to ablation to provide identical ablation for each ablation event. The sample surface was adjusted to be at the focus of a 10× microscope objective lens by moving the stage up and down and monitoring the clearest image of the sample surface through transmitted light and a charge-coupled device (CCD) camera. The objective lens was simultaneously used for focusing the laser beam and imaging the sample surface. The number of laser pulses was controlled by using a Newport electronic shutter driven by a Newport digital exposure control with minimum opening time of 0.01 s. A simple schematic of the laser ablation system is shown in Figure 1. Crater depths were measured using a polarizing light microscope (50× magnifications, Olympus BX51) equipped with a Prior® computer-controlled xyz stage. Surface morphology was studied by SEM (Quanta FEG). Crater diameters were measured from the SEM images using Scandium image processing software.

RESULTS AND DISCUSSIONS

Figure 2 shows a CCD camera image (top view) taken during fs-LA of brass in ambient air. The laser beam was imaged by using a 6 mm pinhole and 10× objective lens and was fired at a repetition rate of 100 Hz and energy of 0.1 mJ to create holes in 4 mm thick brass. Intense light is observed due to the interaction of the laser beam with the sample surface and ejected ablated material. The fluence F (energy per unit area) was calculated using the equation $F = \frac{E}{\pi r^2}$ Where E is the energy in Joules and r is the radius of the crater in cm. Figure 3 shows the dependence of ablation depth on the number of laser pulses in the fluence range 1.14–24.89 J/cm^2 that correspond to an energy range of 0.05 to 0.47 mJ. Ablation depth was calculated as the average of the measured depths of three different craters produced using the same number of laser pulses. As the number of laser pulses increases (>60 pulses at fluence higher than 12.21 J/cm^2), ablation depth becomes too deep (>40 μm) to be measured by the optical microscope used. There is a linear relation between the number of pulses and ablation depth with correlation coefficient R^2 better than 0.9 during the first 50 pulses.

The ablation rate (defined here as the ablation depth per pulse, μm/pulse) was obtained from the slopes of Figure 3 and was found to depend on the laser fluence (see Fig. 4). For fluence lower than 12.21 J/cm^2, there was a rapid increase in the ablation rate (from 83 to 604 nm/pulse) in the fluence range from 1.14 to 12.21 J/cm^2. At fluence higher than 12.21 J/cm^2, the ablation rate increased slowly to reach a maximum of 607 nm/pulse at 19.14 J/cm^2, and then decreased at fluence higher than 19.14 J/cm^2 to 564 nm/pulse at 24.89 J/cm^2. The drop in the ablation rate at fluence >19.14 J/cm^2 may be related to the production of more ablated material that interacts with the incident

https://doi.org/10.1017/S0263034612000407 Published online by Cambridge University Press

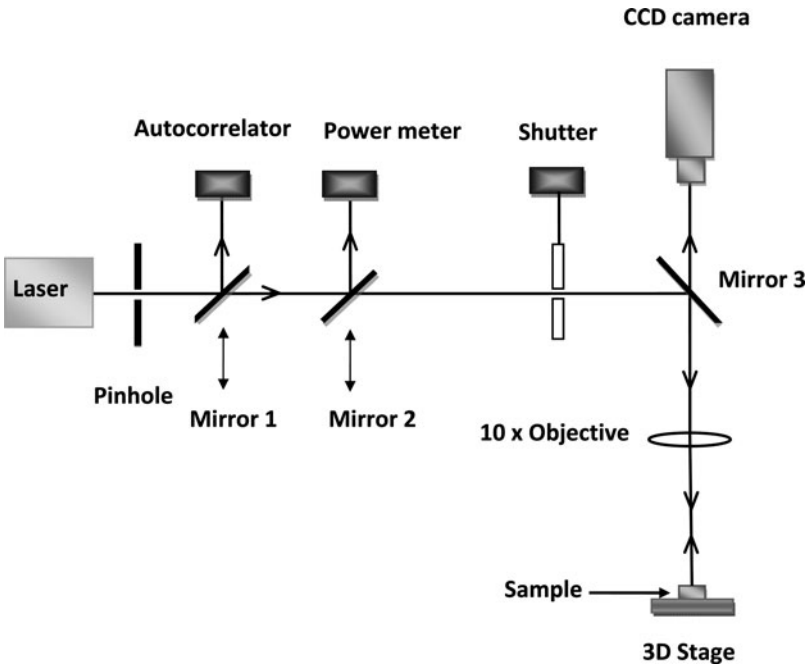

Fig. 1. A simple schematic of the LA system. The laser is focused on the sample surface by using a 10× objective lens. Pulse width and laser power can be measured by reflecting the laser beam into an autocorrelator and a power meter using mirrors 1 and 2, respectively. The number of laser pulses is controlled by a fast electronic shutter. A CCD camera is used to image the sample surface through the 10× objective lens and dichroic mirror 3.

laser beam causing a reduction of energy coupling to the sample. Another possible reason for this reduction in the ablation rate could be attributed to changes in the ablation mechanisms (from non-thermal to thermal) at higher fluence as can be seen from SEM micrographs (Fig. 5) where large droplets of molten material started to appear. Figures 6a and 6b shows the dependence of crater diameter on the number of laser pulses and fluence, respectively. Crater diameters were calculated by taking the average of the measured diameters of three different craters produced using the same number of laser pulses. The crater diameter increases slowly with the number of laser pulses and reaches almost a constant value after a certain number of pulses (depending on the fluence, i.e., about 40, 60, and 70 pulses at 24.89, 19.14, and 1.14 J/cm^2, respectively). The increase of crater diameter with number of pulses and fluence reflects the Gaussian energy distribution of the laser beam. The ablation characteristics of brass in the fluence range 1.14–24.89 J/cm^2 are summarized in Table 1. Due to the Gaussian laser beam energy profile of the femtosecond laser used, a cone-like crater shape was assumed in calculations of crater volumes using the formula: volume = $(h\pi r^2/3)$ where r is the radius of the crater and h is the ablation depth. The mass of material ablated per pulse was calculated by multiplying the crater volume by the brass density (8.5 g/cm^3).

Various effects of femtosecond laser interaction with brass can be observed by inspecting the SEM images of the ablation craters. Figure 7 shows SEM micrographs of some holes drilled through the brass sample at fixed number of laser

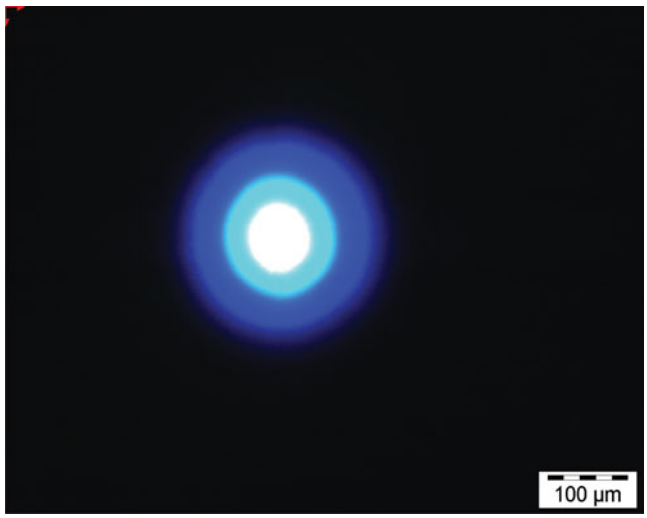

Fig. 2. (Color online) A CCD camera image (top view) of the plasma produced during fs-LA of brass. The laser beam was imaged by using a 6 mm pinhole and 10× objective lens and was fired at repetition rate of 100 Hz and energy of 0.1 mJ. The formation of laser-induced plasma affects the ablation quality and downgrades the advantages of fs-LA.

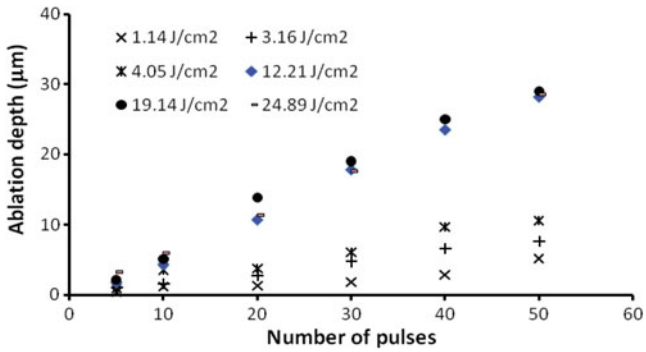

Fig. 3. (Color online) The dependence of ablation depth on the number of laser pulses at different fluence.

https://doi.org/10.1017/S0263034612000407 Published online by Cambridge University Press

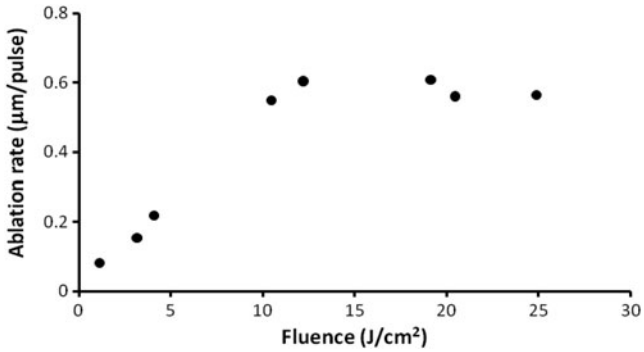

Fig. 4. The dependence of ablation rate on laser fluence.

pulses and variable laser fluence (Fig. 7a–7c) and fixed fluence and variable number of laser pulses (Fig. 7d–7f). The surface morphology and the amount of material ablated and deposited around the craters depend on the laser fluence and number of accumulated pulses. The surface is modified by the first few pulses and then craters start to develop with increasing the numbers of pulses by removing the target material at the irradiation region. Material removal by laser ablation includes several mechanisms (depending on laser and material characteristics) such as Coulomb explosion, ultrafast melting, phase explosion, thermal vaporization, and photomechanical fragmentation (Shank *et al.*, 1983; Rousse *et al.*, 2001; Stoian *et al.*, 2000; Perez & Lewis, 2002; Bulgakova & Bourakov, 2002; Tamura *et al.*, 2001). At low laser fluence ($<19.14\ J/cm^2$), reduced thermal effects can be observed from the edges of the craters, and the material deposited around them as shown in Figure 7. At a small number of laser pulses (depending on the fluence), the craters show defined edges with little debris and particles deposited around them. As the number of pulses increases, substantial build-up of material around and inside the crater takes place. This ablation behavior is different from that of nanosecond laser ablation where thermal processes are the dominant mechanisms of ablation. In nanosecond laser

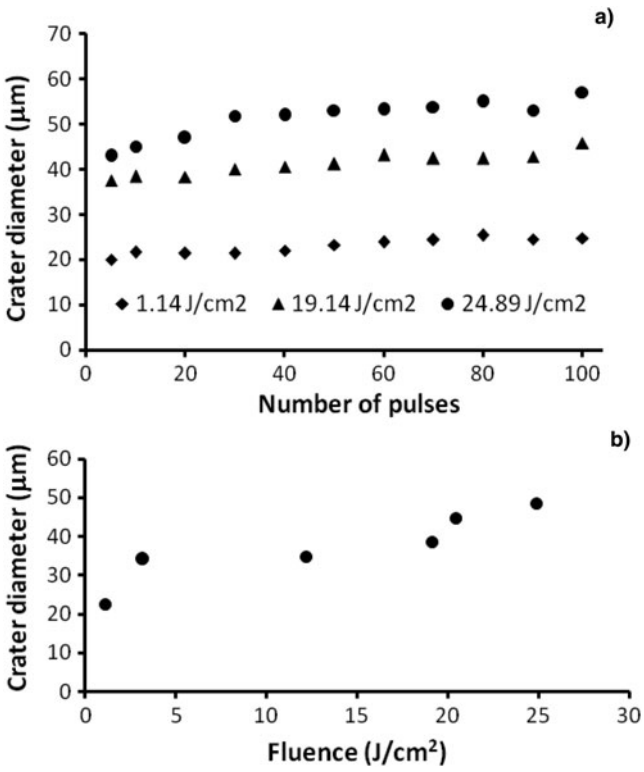

Fig. 6. Dependence of crater diameter on number of pulses (**a**) and fluence (**b**).

ablation of brass, substantial melting, and ejection of large droplets of molten material can be easily observed in Figure 8 where SEM images of a crater produced by 40 ns laser pulses (Nd:YAG, wavelength: 266 nm and pulse width: 8 ns) is shown. The craters have high rims of re-solidified molten material and large particles (in the micrometer range) scattered around them. Comparison between Figure 5 and Figure 8 may not be fair as the ablation conditions (number of laser pulses, fluence and repetition rate) are not identical but it shows some kind of similarity, at a certain point,

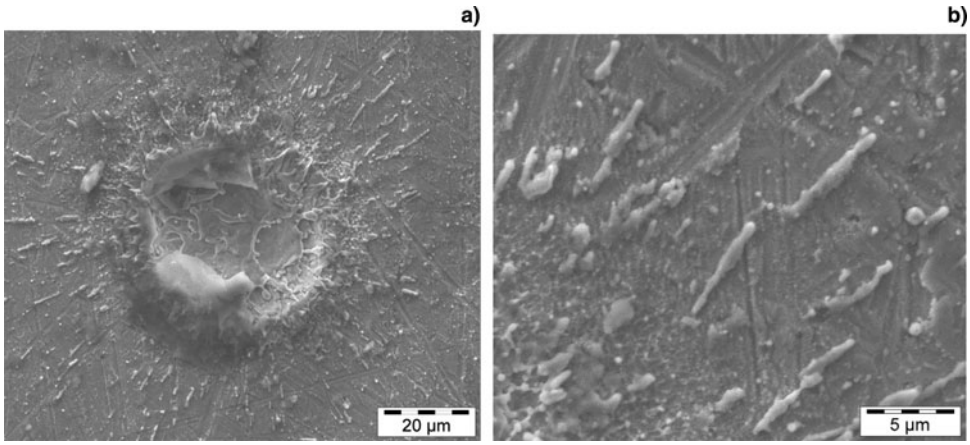

Fig. 5. SEM micrographs of a crater produced by 10 femtosecond laser pulses at $24.89\ J/cm^2$ (**a**) and a close up image of the particles deposited around the crater (**b**). Hydrodynamic effects like formation of re-solidified droplets of the target material appear.

https://doi.org/10.1017/S0263034612000407 Published online by Cambridge University Press

Table 1. *Ablation characteristics of brass at different laser fluence*

Fluence J/cm^2	Power density W/cm^2	Ablation rate μm/pulse	Crater diameter μm	Volume μm^3/pulse	Mass μg/pulse
1.14	114	0.083	22.4	10.9	0.09
3.16	316	0.155	34.2	47.3	0.40
12.21	1221	0.604	34.6	189.7	1.61
19.14	1914	0.607	38.5	235.8	2.00
20.47	2047	0.56	44.6	291.8	2.48
24.89	2489	0.564	48.3	344.4	2.93

between femtosecond and nanosecond laser ablation. In fs-LA, the amount of ablated material increases with increasing laser fluence. Most of the ablated material consists of nanoparticles agglomerated together to form large aggregates as shown in Figure 9. A few spherical particles with diameters smaller than 400 nm can be seen embedded in the ablation debris. At high fluence (>20.47 J/cm^2) hydrodynamic effects like formation of re-solidified droplets of materials appear as shown in Figure 5 where a crater produced by fs laser ablation (10 pulses) of brass is shown. These effects look similar to those produced by nanosecond laser ablation (Figure 8) and may be a reason for the reduction in the

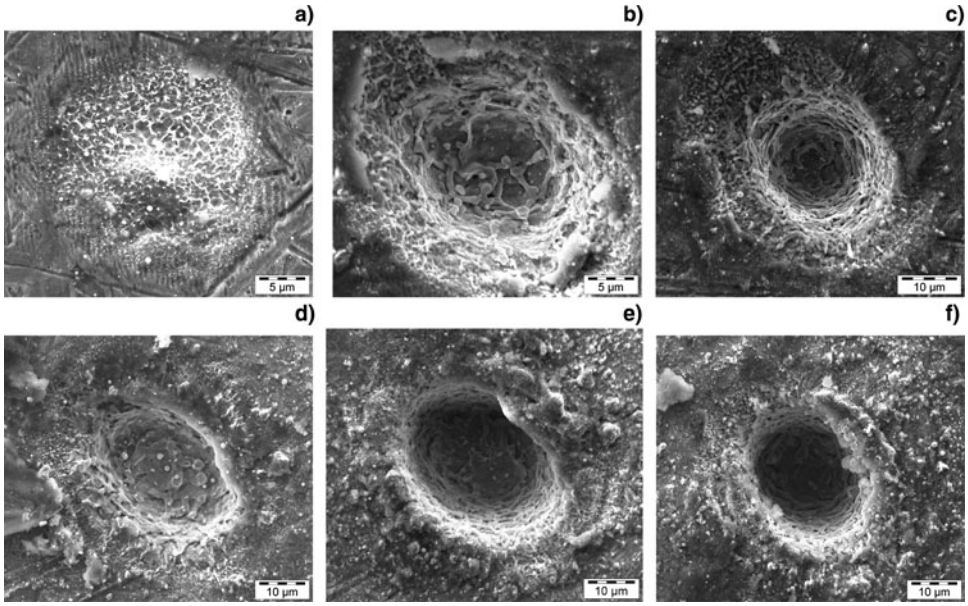

Fig. 7. SEM micrographs of craters produced by fs-LA at different fluence and numbers of laser pulses; (**a**–**c**) 60 pulses at 1.14 J/cm^2, 3.16 J/cm^2 and 4.08 J/cm^2, respectively; (**d**–**f**) 30, 60, and 80 pulses, respectively, at constant fluence of 10.49 J/cm^2.

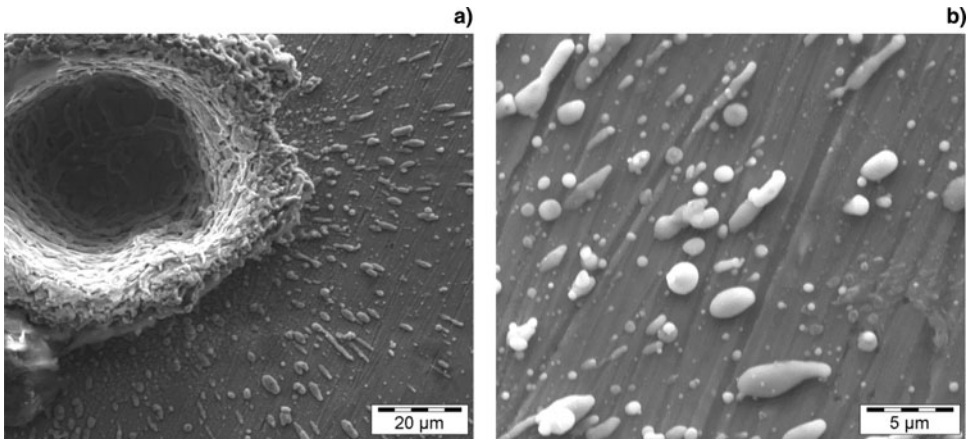

Fig. 8. A crater produced by 40 nanosecond laser pulses (Nd:YAG laser, wavelength 266 nm, pulse width 8 ns) laser ablation (**a**) and a close up image of the particles deposited around the crater (**b**). The images show a high crater rim and re-solidified particles around it, which indicates the thermal nature of nanosecond laser ablation.

https://doi.org/10.1017/S0263034612000407 Published online by Cambridge University Press

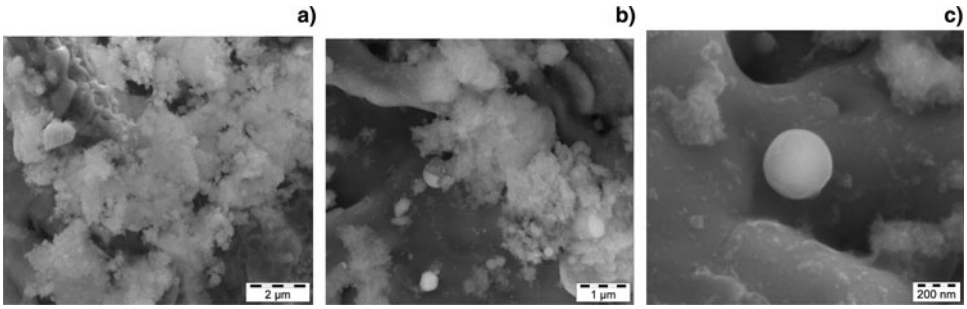

Fig. 9. SEM micrographs of the particles produced by fs laser ablation; (**a**, **b**) agglomeration of fine particles; (**c**) a close up SEM image of a large spherical particle (diameter <400 nm) at the bottom of the crater.

ablation rate at this high fluence, as mentioned previously. The presence of re-solidified μm size particles deposited around the ablated craters indicates a different ablation mechanism where thermal effects control the ablation (Pecholt *et al.*, 2008).

In this work, brass was ablated using femtosecond laser pulses at repetition rate of 100 Hz in ambient air. The ablated material was not removed from the interaction region and was available to interact with the incident laser pulses creating high temperature plasma (Fig. 2) especially at high laser fluence. Zheng *et al.* (2007) estimated the plasma temperature created by fs-LA of brass at energy of 0.26 mJ to be 9205.4 K. The formation of a laser-induced plasma downgrades the advantages of fs-LA by acting as an energy source that supplies heat to the created structures during material processing (Zheng *et al.*, 2007). This laser-induced plasma may interact with the crater walls and absorbs part of the incident laser energy causing possible damage of the crater walls and reduction in the ablation rate. This distortion can be clearly seen in Figure 7b–7c where the top surface at the crater rim is eroded by the action of the laser-induced plasma. The distortion of the crater walls may also be related to the non-uniform heat conduction from the focal spot or crater at the surface of the target material (Anwar *et al.*, 2006). To improve the quality of material processing, the laser operating conditions and the medium in which ablation takes place must be optimized. Using a lower repetition rate and conducting the ablation in a flowing gas with appropriate properties may help to improve the ablation quality by reducing plasma formation and clearing ablated material from the interaction region.

CONCLUSIONS

In this paper we investigated the effect of laser fluence and number of femtosecond laser pulses on ablation rate, crater diameter and surface morphology of brass in ambient air. Laser fluence was found to have a direct effect on the ablation rate and ablation behavior. At fluence $<19.14\ J/cm^2$, material removal involved a transition from solid to vapor phase with the formation of fine particles (in the nanometre range) agglomerated into larger aggregates with minimum droplets from the molten phase. At fluence of $>20.47\ J/cm^2$, material removal was characterized by ejection of droplets of molten material indicating an increase in the thermal effects. For better ablation quality, both laser operating conditions (fluence, repetition rate, and wavelength) and ablation environment gas should be optimized to avoid the formation of laser-induced plasma and its negative consequences on the processed features.

ACKNOWLEDGEMENTS

The authors would like to thank Sharon Lackie for her help during SEM measurements. Support for this research was provided by a National Sciences and Engineering Research Council Discovery Grant to B.J. Fryer. Infrastructure support was provided by CFI/OIT grants to B.J. Fryer and by the University of Windsor.

REFERENCES

Anwar, M.S., Latif, A., Iqbal, M., Rafique, M.S., Khaleeq-ur-Rahman, M. & Siddique, S. (2006). Theoretical model for heat conduction in metals during interaction with ultra short laser pulse. *Laser Part. Beams* **24**, 347–353.

Batani, D. (2010). Short-pulse laser ablation of materials at high intensities: Influence of plasma effects. *Laser Part. Beams* **28**, 235–244.

Bonse, J., Baudach, S., Kruger, J., Kautek, W. & Lenzner, M. (2002). Femtosecond laser ablation of silicon-modification thresholds and morphology. *Appl. Phys. A Mater. Sci. Process*. **74**, 19–25.

Bonse, J., Wrobel, J.M., Kruger, J. & Kautek, W. (2001). Ultrashort pulse laser ablation of indium phosphide in air. *Appl. Phys. A Mater. Sci. Process*.**72**, 89–94.

Bulgakova, N. & Bourakov, I. (2002). Phase explosion under ultrashort pulsed laser ablation: modeling with analysis of metastable state of melt. *Appl. Surf. Sci*. **197–198**, 40–45.

Choi, T.Y. & Grigoropoulos, C.P. (2002). Plasma and ablation dynamics in ultrafast laser processing of crystalline silicon. *J. Appl. Phys*. **92**, 4918–4925.

Couillard, M., Borowiec, A., Haugen, H.K., Preston, J.S., Griswold, E.M. & Botton, G.A. (2007). Subsurface modifications in indium phosphide induced by single and multiple femtosecond laser pulses: a study on the formation of periodic ripples. *J. Appl. Phys*. **101**, 033519, doi:10.1063/1.2407259.

Coyne, E., Magee, J.P., Mannion, P., O'Connor, G.M. & Glynn, T.J. (2005). STEM (scanning transmission electron microscopy) analysis of femtosecond laser pulse induced damage to bulk silicon. *Appl. Phys. A Mater. Sci. Process*. **81**, 371–378.

Di Bernardo, A., Courtois, C., Cros, B., Matthieussent, G., Batani, D., Desai, T., Strati, F. & Lucchini, G. (2003). High-intensity ultrashort laser-induced ablation ofstainless steel foil targets in the presence of ambient gas. *Laser Part. Beams* **21**, 59–64.

Fang, R., Zhang, D., Wei, H., Li, Z., Yang, F. & Gao, Y. (2010). Improved two-temperature model and its application in femtosecond laser ablation of metal target. *Laser Part. Beams* **28**, 157–164.

Freydier, R., Candaudap, F., Poitrasson, F., Arbouet, A. & Chatel, B. Dupre, B. (2008). Evaluation of infrared femtosecond laser ablation for the analysis of geomaterials by ICP-MS. *J. Anal. At. Spectrom*. **23**, 702–710.

Fernandez, B., Claverie, F., Pecheyran, C. & Donard, O.F.X. (2007). Direct analysis of solid samples by fs-LA-ICP-MS. *Trends Anal. Chem*. **26**, 951–966.

Horn, I. & von Blanckenburg, F. (2007). Investigation on elemental and isotopic fractionation during 196 nm femtosecond laser ablation multiple collector inductively coupled plasma mass spectrometry. *Spectrochim. Acta Part B* **62**, 410–422.

Ikehata, K., Notsu, K. & Hirata, T. (2008). In situ determination of Cu isotope ratios in copper-rich materials by NIR femtosecond LAMC-ICP-MS. *J. Anal. At. Spectrom*. **23**, 1003–1008.

Ji, L.F., Li, L., Devlin, H., Liu, Z., Whitehead, D., Wang, Z.B., Wang, W. & Jiao, J. (2011). Ti: sapphire femtosecond laser interaction with human dental dentine. *Sur. Eng*. **27**, 749–753.

Kanavin, A.P., Smetanin, I.V., Isakov, V.A. & Afanasiev, Y.V. (1998). Heat transport in metals irradiated by ultrashort laser pulses. *Phys. Rev. B*. **57**, 14698.

Kumar, A. & Verma, A.L. (2011). Nonlinear absorption of intense short pulse laser over a metal surface embedded with nanoparticles. *Laser Part. Beams* **29**, 333–338.

Latif, A., Anwar, M.S., Aleem, M.A., Rafique, M.S. & Khaleeq-Ur-Rahman, M. (2009). Influence of number of laser shots on laser induced microstructures on Ag and Cu targets. *Laser Part. Beams* **27**, 129–136.

Lenzner, M., Kruger, J., Sartania, S., Cheng, Z., Spielmann, C., Mourou, G., Kautek, W. & Krausz, F. (1998). Femtosecond Optical Breakdown in Dielectrics. *Phys. Rev. Let*. **80**, 4076–4079.

Liu, Y.F. & Niemz, M. (2007). Ablation of femural bone with femtosecond laser pulses – a feasibility study. *Lasers Med. Sci*. **22**, 171–174.

Menendez-Manjon, A., Barcikowski, S., Shafeev, G.A., Mazhukin, V.I. & Chichkov, B.N. (2010). Influence of beam intensity profile on the aerodynamic particle size distributions generated by femtosecond laser ablation. *Laser Part. Beams* **28**, 45–52.

Neev, J., Da Silva, L.B., Feit, M.D, Perry, M.D., Rubenchik, A.M. & Stuart, B.C. (1996). Ultrashort pulse laser system for hard dental tissue procedures. Lasers in dentistry II: San Jose CA, 28–29 January 1996. *Proc. SPIE-Int. Soc. Opt. Eng*. 210–221.

Niemz, M.H., Kasenbacher, A., Strassl, M., Backer, A., Beyertt, A., Nickel, D. & Giesen, A. (2004). Tooth ablation using a CPA-free thin disk femtosecond laser system. *Appl. Phys. B Lasers Opt. Print*. **79**, 269–271.

Niemz, M.H. (1998). Ultrashort laser pulses in dentistry: advantages and limitations. Applications of ultrashort-pulse lasers in medicine and biology: San Jose CA, 29–30 January 1998. *Proc. SPIE-Int. Soc. Opt. Eng*. 84–91.

Pecholt, B., Vendan, M., Dong, Y. & Molian, P. (2008). Ultrafast laser micromachining of 3C-SiC thin filmsfor MEMS device fabrication. *Int. J. Adv. Manuf. Technol*. **39**, 239–250.

Perez, D. & Lewis, L. (2002). Ablation of solids under femtosecond laser pulses. *Phys. Rev.Lett*. **89**, 25504.

Perrie, W., Gilla, M., Robinson, B., Foxa, P. & O'Neil, W. (2004). Femtosecond laser micro-structuring of aluminum under helium. *Appl. Surf. Sci*. **230**, 50–59.

Poitrasson, F., Mao, X.L., Mao, S.S., Freydier, R. & Russo, R.E. (2003). Comparison of ultraviolet femtosecond and nanosecond laser ablation inductively coupled plasma mass spectrometry analysis in glass, monazite, and zircon. *Anal. Chem*. **75**, 6184–6190.

Robinson, G.M. & Jackson, M.J. (2006). Femtosecond laser machiningof aluminum surfaces under controlled gas atmospheres. *J. Mater. Eng. Perform*. **15**, 155–159.

Rousse, A., Rischel, C., Fourmaux, S., Uschmann, I., Sebban, S., Grillon, G., Balcou, P., Förster, E., Geindre, J., Audebert, P., Gauthier, J. & Hulin, D. (2001). Non-thermal melting in semiconductors measuredat femtosecond resolution. *Nature* **410**, 65–68.

Russo, R.E., Mao, X. & Mao, S.S. (2002). The physics of laser ablation in micro chemical analysis. *Anal. Chem*. **74**, 70A–77A.

Shaheen, M.E. & Fryer, B.J. (2011). A simple solution to expanding available reference materials for Laser Ablation Inductively Coupled Plasma Mass Spectrometry analysis: Applications to sedimentary materials, *Spectrochim. Acta Part B* **66**, 627–636.

Shank, C., Yen, R. & Hirlimann, C. (1983). Femtosecond-timeresolvedsurface structural dynamics of optically excited silicon. *Phys. Rev. Lett*. **51**, 900–902.

Stasic, J., Gakovic, B., Krmpot, A., Pavlovic, V., Trtica, M. & Jelenkovic, B. (2009). Nickel-based super-alloy Inconel 600 morphological modifications by high repetition rate femtosecondTi:sapphire laser. *Laser Part. Beams* **27**, 85–90.

Stoian, R., Ashkenasi, D., Rosenfeld, A. & Campbell, E. (2000). Coulomb explosion in ultrashort pulsed laser ablation of Al203. *Phys. Rev. B* **62**, 13167–13172.

Sun, J. & Longtin, J.P. (2001). Inert gas beam delivery for ultrafast laser micromachining at ambient pressure. *Appl. Surf.Sci*. **89**, 8219–8223.

Tamura, H., Kohama, T., Kondo, K. & Yoshida, M. (2001). Femtosecond laser-induced spallation in aluminum. *J. Appl. Phys*. **89**, 3520–3522.

Zheng, H.Y., Deng, Y.Z., Vatsya, S.R. & Nikumb, S.K. (2007). A study of balancing the competing effects of ultrashort laser induced plasma for optimal laser machining. *App. Sur. Sci*. **253**, 3408–3412.

Zhu, X., Naumov, A.Yu., Villeneuve, D.M. & Corkum, P.B. (1999). Influence of laser parameters and material properties on micro drilling with femtosecond laser pulses. *Appl. Phys. A* **69**, S367–S371.